

Manufacturing Dissolvable Alloy Components using ShAPE

A Study on Solid Phase Processing of
Mg-W Composites and WJ11 Alloys

September 2021

Jens Darsell
Dalong Zhang
Nicole Overman
Nathan Canfield
Timothy Roosendaal
Keerti Kappagantula

DISCLAIMER

This report was prepared as an account of work sponsored by an agency of the United States Government. Neither the United States Government nor any agency thereof, nor Battelle Memorial Institute, nor any of their employees, **makes any warranty, express or implied, or assumes any legal liability or responsibility for the accuracy, completeness, or usefulness of any information, apparatus, product, or process disclosed, or represents that its use would not infringe privately owned rights.** Reference herein to any specific commercial product, process, or service by trade name, trademark, manufacturer, or otherwise does not necessarily constitute or imply its endorsement, recommendation, or favoring by the United States Government or any agency thereof, or Battelle Memorial Institute. The views and opinions of authors expressed herein do not necessarily state or reflect those of the United States Government or any agency thereof.

PACIFIC NORTHWEST NATIONAL LABORATORY
operated by
BATTELLE
for the
UNITED STATES DEPARTMENT OF ENERGY
under Contract DE-AC05-76RL01830

Printed in the United States of America

Available to DOE and DOE contractors from
the Office of Scientific and Technical
Information,
P.O. Box 62, Oak Ridge, TN 37831-0062
www.osti.gov
ph: (865) 576-8401
fox: (865) 576-5728
email: reports@osti.gov

Available to the public from the National Technical Information Service
5301 Shawnee Rd., Alexandria, VA 22312
ph: (800) 553-NTIS (6847)
or (703) 605-6000
email: info@ntis.gov
Online ordering: <http://www.ntis.gov>

Manufacturing Dissolvable Alloy Components using ShAPE

A Study on Solid Phase Processing of Mg-W Composites and WJ11 Alloys

September 2021

Jens Darsell
Dalong Zhang
Nicole Overman
Nathan Canfield
Timothy Roosendaal
Keerti Kappagantula

Prepared for
the U.S. Department of Energy
under Contract DE-AC05-76RL01830

Pacific Northwest National Laboratory
Richland, Washington 99354

Table of Contents

| | |
|---------------------------------------|----|
| Executive Summary | 3 |
| 1.0 Introduction..... | 4 |
| 2.0 Materials and Methods | 5 |
| 3.0 Results & Discussion | 7 |
| 3.1 Microstructural Analysis | 7 |
| 3.2 Processing Conditions | 14 |
| 3.3 Mechanical Performance | 14 |
| 4.0 Conclusions and Future Work | 17 |
| References | 18 |

Executive Summary

Dissolvable alloys and composites are an emerging class of materials that demonstrate tailored sorptivity in corrosive environments. This work explored the viability of solid phase processing (SPP) techniques, namely the shear assisted processing and extrusion (ShAPE™) method, to manufacture dissolvable magnesium composites and alloys components such as rods and tubes. The study also determined the effects of material composition and manufacturing process conditions on material microstructures developed during SPP and the resulting performance of the components. Explicit properties of interest included ultimate tensile strength, ultimate compressive strength, and yield strength.

The application fields of interest for dissolvable alloys were identified as oil-and-gas operations and biomedical implants. Accordingly, PNNL collaborated with industrial and academia partners, Fortek Industries, Houston and University of Pittsburgh, during the course of this project for material and ShAPE process development. PNNL determined the viability of the using ShAPE to process the custom-designed materials provided by the project partners. This was done by identifying process parameters such as tool rotation rate, tool plunge rate, and process cooling optimal for manufacturing components with consolidated microstructures. Subsequently, PNNL also performed microstructural characterization on unprocessed and processed samples and mechanical property testing.

One of the major findings from this work is that ShAPE was able to manufacture dissolvable magnesium composite and alloy rods and tubes with consolidated homogeneous microstructures and minimal macroscale defects on component surfaces. It was observed that samples processed via ShAPE demonstrated an average grain size $< 2 - 5 \mu\text{m}$, which was markedly lower than that of the precursors with $8 - 13 \mu\text{m}$ grains. Results showed that the ShAPE synthesized dissolvable magnesium composite and alloy strength was on par with or better than those components that were manufactured using traditional manufacturing processes such as forging and extrusion. It is noteworthy that the ShAPE samples were made with considerably lower number of process steps.

This report provides comprehensive information on the activities and outcomes derived during the course of this project. Section 1 of this report provides an introduction and background information on dissolvable alloys, their applications and the necessity of advanced manufacturing processes such as ShAPE in advancing their commercialization activities. In Section 2, manufacturing, characterization, and testing methodologies used in this study are discussed. Section 3 provides information on the results and a discussion on microstructure feature and performance trends. Section 4 discusses the conclusions drawn from this work and potential future work.

1.0 Introduction

Dissolvable alloys and composites are materials that are deployed in corrosive environments to perform specific activities such as provide structural support, act as heat sinks, or enable component separation during operations. At the end of their performance period, these materials with tailored compositions and microstructures are designed to be consumed by the environment entirely. As such, dissolvable material components are used typically in applications where component retrieval after the period of performance is highly challenging, resource-intensive and otherwise detrimental to the system performance. Their deployment is of interest to oil-and-gas operations and as orthopedic and cardiovascular implants. Dissolvable alloy and composite components find widespread applications as valve seats, pipe scrapers, clamps, and high pressure frac-balls; they are also used to make orthopedic and cardiovascular implants such as rods, pins, and stents.

In the past decade, several magnesium (Mg) alloys, including but not limited to rare-earth containing ones like WE43, Mg-Zn-Ca based alloys and Mg based metal matrix composites have been identified as ideal dissolvable alloy and composite materials [1], [2]. Controlled dissolvability is achieved in such material systems through prudent alloying element choices. However, for dissolvable alloy and composite material components to demonstrate the requisite mechanical and sorptive performance, two factors are essential: (a). the second phases, additives or alloying inclusions must be distributed uniformly in the microstructure; and (b). material microstructure must demonstrate small grain sizes.

Both these conditions can be accomplished when materials are processed using solid phase processing (SPP) techniques such as equal-channel angular pressing (ECAP) [3] and high pressure torsion (HPT) [4] which refine the grain size to 1~2 μm . However, these processes do not have the necessary high throughput and are prohibitively expensive on a commercial scale. Forming such materials into relevant profiles at industrially viable volumes, while achieving the essential microstructural features and bulk scale performance remains a challenge [5]. In general, Mg alloys and composites cannot be extruded easily due to their propensity for developing surface tears and low ductility; they also form large grains and second-phase stringers inherent to Mg extrusions [6]. On the other hand, Mg alloy corrosion resistance and mechanical performance improves with decreasing grain size and homogeneously distributed second phases in the microstructure [7]. While the alloy formulation development has reached maturity, commercialization is severely limited by their manufacturability and associated costs.

The patented shear assisted processing and extrusion (ShAPETM) developed at PNNL is an SPP method predicted on friction extrusion. ShAPE can refine metal microstructures by decreasing the average grain size as well as homogeneously distribute the second phase particles [8]. These features have been correlated to enhanced mechanical performance and more uniform corrosion behavior. More importantly, ShAPE provides a scalable, low-energy low-carbon route for manufacturing dissolvable alloy and composite components compared to the currently used bench-scale high strain processing methods. At this stage of development, it is essential to understand the property evolution when the Mg dissolvable alloys and composites are subjected to high strain, far-from-equilibrium processing conditions afforded by ShAPE. In this project, research tasks were performed to address the technical challenges which are currently identified as barriers for the commercialization of Mg dissolvable alloy and composite components.

2.0 Materials and Methods

Custom-designed Mg dissolvable composites with 4 wt.% and 5 wt.% tungsten (W) were provided by Fortek Inc., TX (Fortek) and will be referred to as Mg-4W and Mg-5W respectively, in this report. Dissolvable Mg alloy, WJ11, was provided to PNNL by University of Pittsburgh (UPitt) at no cost to project. WJ11 was designed for orthopedic implant applications and has strontium (Sr), Yttrium (Y) and zirconium (Zr) among other elements as second phase alloying additions in the Mg matrix. Mg-4W and Mg-5W billets were manufactured by hot-forging the constituent Mg alloy and second phase additive powders by Fortek. On the other hand, the WJ11 billets were cast by external collaborators and provided to PNNL by UPitt. In addition, UPitt also provided hot-extruded WJ11 rods for microstructural characterization; these rods were synthesized with an extrusion ratio of 10.

ShAPE tools were manufactured using H13 steel. The rod-tool and tube-tool had internal diameters of 5 mm and 7.5 mm respectively. A mandrel was manufactured, also using H13 steel, with an outer diameter of 6 mm to be incorporated co-axially with the tube-tool to manufacture tubes with a wall thickness of 1.5 mm. All the tools had four scrolls on the die-face.

A process schematic is shown in Figure 1 which depicts equipment configurations utilized to extrude tube versus rod geometries. To manufacture the rods and tubes, requisite tools were fixed to the spindle of the ShAPE equipment, and a container holding the billet was attached to the tailstock. ShAPE was performed with a custom-designed die and material container assembly that was loaded into and actuated using a Friction Stir Welding (FSW) machine designed and built by Bond Technologies (previously named Transformation Technologies Incorporated). This FSW machine is unique in that it is a servo-operated machine capable of an axial force up to 130 kN and uses a nominally rated 30kW spindle that can operate up to 2000 rpm. In addition, it is fully instrumented to record forces in the x, y and z directions as well as torque, power, and temperature.

To manufacture the rods and tubes, requisite tools were fixed to the spindle of the ShAPE equipment, and a container holding the billet was attached to the tailstock. During ShAPE, a rotating tool impinges on a stationary billet. Due to the friction experienced at the tool/die interface and the mechanical work applied, the billet plasticizes without melting and eventually exits the processing zone through the die cavity to form the extrudate. Process cooling was provided by helium gas impinging on the tooling at specific volumetric rates. In this work, the force in the z-direction corresponds to the axial forge force and will be the only force discussed further. Die face temperature was recorded by inserting a type-K thermocouple approximately 1-2mm from the working face of the die.

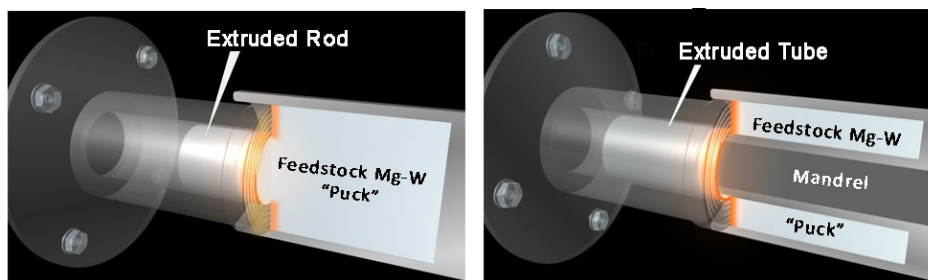


Figure 1. Processing schematics for the fabrication of (a). rod and (b). tube using ShAPE technology. The diagrams show Mg-W pucks as representative billet material.

An initial parametric study was performed to identify the ShAPE tool rotation rate, tool plunge rate, and cooling conditions required to manufacture Mg-4W, Mg-5W and WJ11 rods and tubes using ShAPE. After the initial testing, it was seen that macroscopically defect free Mg-4W, Mg-5W and WJ11 rods were manufactured at temperatures between 370 – 400 °C while a higher temperature range of 420 – 450 °C was more suitable for the tube manufacturing.

Multiple nanoanalysis techniques were utilized to assess microstructural characteristics of the Mg alloys and composites before and after ShAPE to evaluate the effect of the processing parameters on the grain and second phase morphology. Electron backscatter diffraction (EBSD) was used to obtain grain size of the Mg matrix. A combination of secondary electron (SE), low angle backscatter electron (BSE) and forescatter diode (FSD) imaging was used to visualize the size and distribution of second phases. Scanning electron microscopy was performed using a JEOL 7600 field-emission scanning electron microscope equipped with Oxford's 170 mm² Ultim MAX energy dispersive spectroscopy (EDS) detector and a Symmetry EBSD camera. EBSD was performed using the AZtec NanoAnalysis Software, version 4.1. EBSD mapping was accomplished with an accelerating voltage of 20 kV, a specimen tilt of 70.0°, and a working distance of ~24 mm and was limited to mapping of the Mg matrix. Indexing of the Mg matrix phase was performed using a hexagonal crystal system, space group (194), Laue group (6/mmm) with lattice parameters $a = b = 3.2089 \text{ \AA}$; $c = 5.2101 \text{ \AA}$, and $\alpha = \beta = 90^\circ$ with $\gamma = 120^\circ$. A 170 mm² Ultim MAX detector was used for EDS measurement, which was performed at an accelerating voltage of 5 kV. Following acquisition of EBSD data, post-processing (wild spike elimination and a medium level of zero solution extrapolation) was performed using the HKL Technology Channel5 Tango software. Grain size statistics reported were generated solely from the Mg matrix phase. Grain size was evaluated using the linear intercept method, with border grains removed from the data set. Grain differentiation was performed using a boundary misorientation of 8 degrees. Transmission electron microscopy (TEM) samples were prepared using a Thermo Fisher Scientific Quanta 3D focus ion beam (FIB) scanning electron microscope (SEM). FIB lamellae were extracted using a 30 keV Ga beam for the initial lift-out and thinning. Samples were then thinned down to ~100 – 200 nm using a 5 KeV beam followed by a 2 keV step.

The mechanical testing and samples were prepared as per ASTM E8 standard with a 3 mm gauge diameter. Tensile and compression specimens were machined with the gauge length along the extrusion direction for extruded rods. Tensile and compression tests were performed at room temperature with a quasi-static strain rate of 10⁻³/s. Digital image correlation (DIC) was also used for tensile tests to accurately determine the strain values.

3.0 Results & Discussion

3.1 Microstructural Analysis

BSE images of the as received Mg-4W and Mg-5W are shown in Figure 2 exhibiting significant heterogeneity. Grain boundaries are decorated with W-rich particles (bright white contrast) and were also observed to exhibit oxygen enrichment (darker contrast along boundaries). As a result, grain boundary traces were readily visible and suggest a maximum grain size on the order of $\sim 100\ \mu\text{m}$. At elevated magnification, additional submicron and refined second phases were observed in the as-received material that exhibited mass contrast in between that of the Mg matrix and W particulate, labeled in Figure 2(d). EDS analysis of the sub-micron refined phases indicated that they were primarily enriched in aluminum (Al) and Mg, with a nominal composition of $\sim 66\ \text{wt.}\%$ Mg and $31\ \text{wt.}\%$ Al with the rest of the material comprising of carbon (C) and oxygen (O). Darker regions in the as-received material were correlated with oxidized portions. The nominal composition of the Mg matrix was identified as $91.3\ \text{wt.}\%$ Mg and $7.7\ \text{wt.}\%$ Al. Under the hot-forging conditions used to manufacture the precursor billets, W particle size ranged widely from $0.84 - 8.57\ \mu\text{m}$ with a mean particle size of $3.11 \pm 1.5\ \mu\text{m}$.

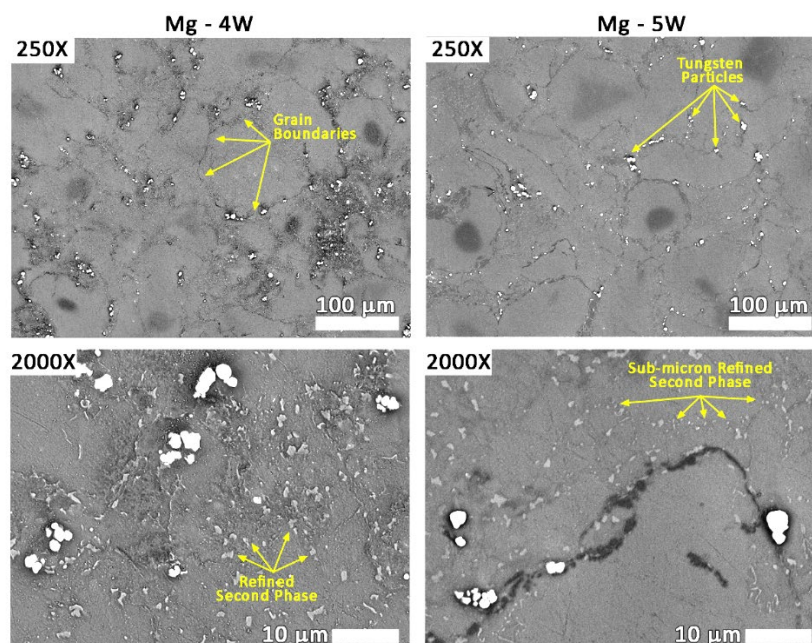


Figure 2. Low accelerating voltage (5kV) backscatter electron images of the as received material microstructures confirm a large grain size and show the presence of considerable refined second phase formation.

EBSD mapping was performed on the as-received hot-forged Mg-4W and Mg-5W composites to quantify grain size and the band contrast maps are shown in Figure 2. Mapping of diffraction pattern quality offers a mechanism for visualizing areas of a given microstructure that deviate from a perfect unstrained Mg crystal. Poor diffraction indexing (darker coloring) was observed along grain boundaries and from areas where non-Mg diffraction (W particles) were present. Additionally, presence of pockets of refined grains in the feedstock material that were not easily distinguished in the BSE images (Figure 2) were also observed in the EBSD contrast maps.

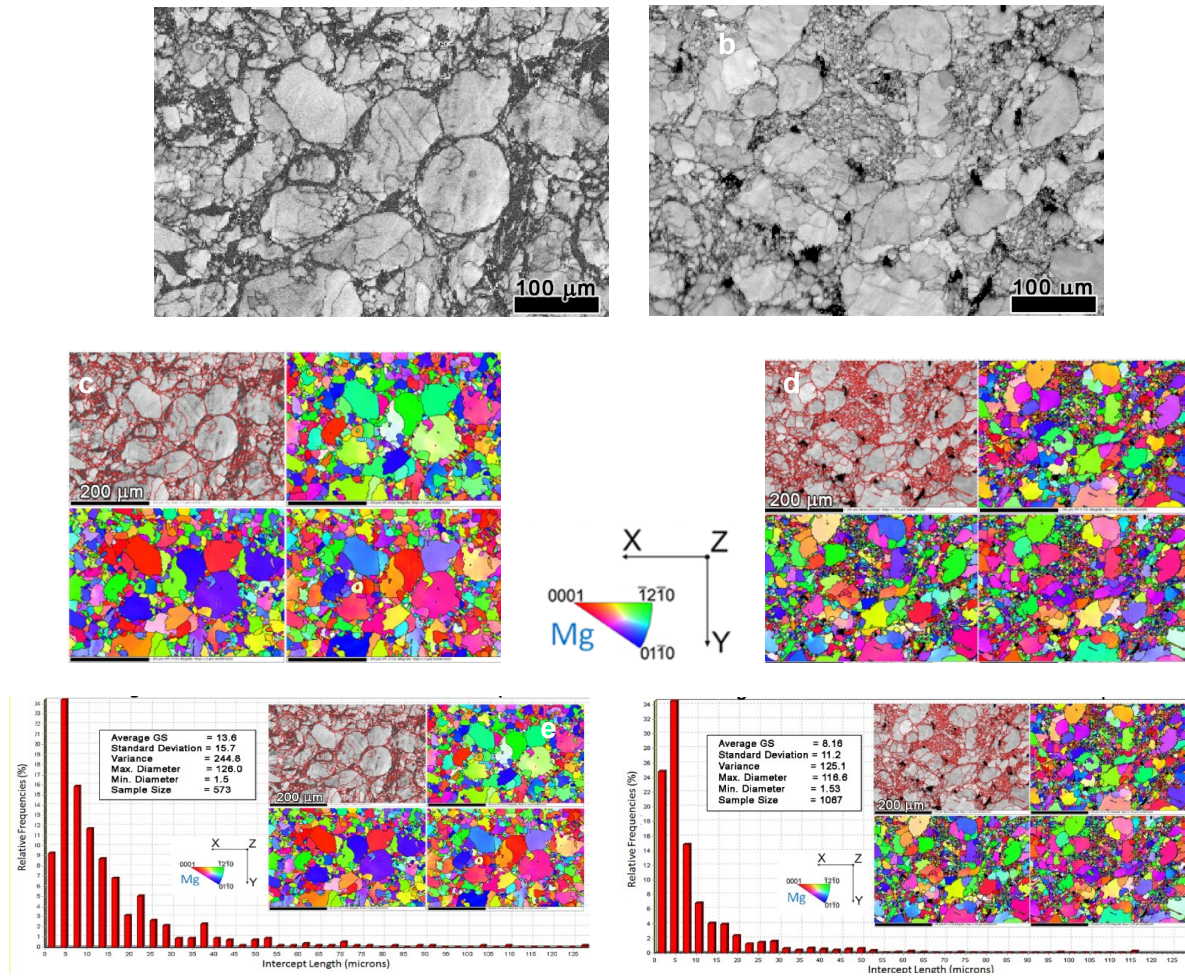


Figure 3. EBSD band contrast maps of the as-received, hot-forged (a). Mg-4W, and (b). Mg-5W billets revealing a Mg matrix grain structure that is comprised of both large (~100 μm) grains and pockets of smaller (~15 μm) grains. Inverse pole figures of (c). Mg-4W and (d). Mg-5W samples in the x-, y-, and z-directions. Grain size distribution histograms with IPFs in the inset for the as-received, hot-forged (e). Mg-4W and Mg-5W composites.

The band contrast maps of as-received Mg-4W and Mg-5W hot-forged billets were used to determine the grain boundary misorientation for grain size determination. A boundary misorientation of 8° was used to distinguish different grains. Table 1 presents the grain size distribution of the Mg matrix. Comparison of the two specimens suggests the Mg-5W sample is more structurally refined than the Mg-4W sample possibly owing to the higher concentration of W which can act as grain pinning sites during hot-forging. Both specimens exhibit a broad range of grain sizes and considerable non-uniformity of grain size.

Table 1. Grain size distribution of the Mg matrix in precursor Mg-W alloys.

| Specimen | Average diameter ± standard error (μm) | Standard Deviation (μm) | Maximum Diameter (μm) | No. of grains sampled |
|----------|--|-------------------------|-----------------------|-----------------------|
| Mg-4W | 13.60 ± 0.656 | 15.7 | 126.0 | 573 |
| Mg-5W | 8.16 ± 0.343 | 11.2 | 125.1 | 1067 |

Figure 3 also presents the inverse pole figure maps in the X, Y, and Z directions and the grain size distribution histograms. Surprisingly, for a Mg alloy, minimal basal texturing was observed in either of the samples in the mapped area. This may be because the samples were hot forged rather than being extruded. If present, a basal texture would have resulted in considerably increased red coloring in the IPF maps.

Low kV backscatter electron imaging of the ShAPE processed Mg-4W tube and Mg-5W rod are presented in Figure 4. The presence of W particulate remains relatively unchanged before and after ShAPE processing. However, the matrix material has undergone significant homogenization with respect to boundary oxidation and refined second phases that were present in the feedstock material. Grain boundaries are no longer easily distinguished and highlighted by the presence of second phases.

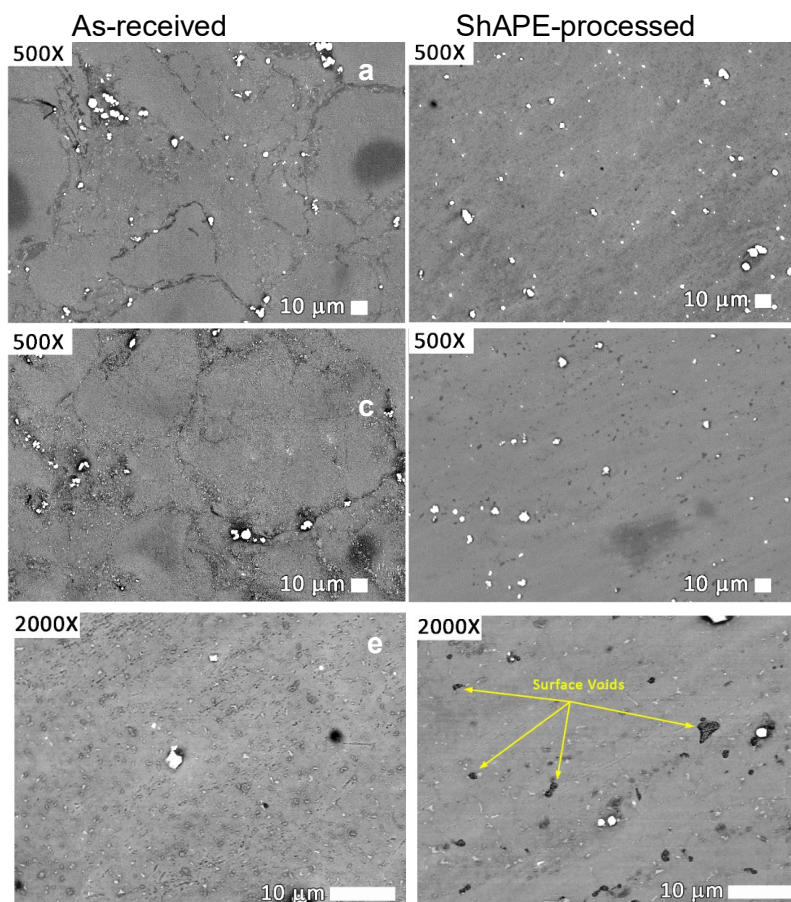


Figure 4. Low accelerating voltage (5kV) backscatter electron images of (a). as-received, hot-forged Mg-4W billet, (b). ShAPE Mg-4W tube, (c). hot-forged, as-received Mg-5W billet, (d). ShAPE Mg-5W rod, (e). ShAPE Mg-4W tube, (f). Mg-5W rod microstructures. The sample matrix has undergone significant homogenization, while tungsten particle size and distribution appears largely unaltered.

Higher magnification imaging further highlights Mg matrix homogenization. High resolution EBSD analysis of any potential metastable or intermetallic phases was not performed at this point, as these secondary particulates exhibited a level of structural refinement better suited to analysis and identification using transmission electron microscopy, which is beyond the scope of the current project.

EBSD mapping was utilized to quantify grain size reduction in the ShAPE processed Mg-4W and Mg-5W samples. The processed material was evaluated in two locations, in the puck specimen nearest the transition region to evaluate an early/intermediate position during processing, and in the center of a fully processed tube/rod extrudate. A summary of the grain size evaluations performed is shown in Table 2. Associated EBSD band contrast maps with grain boundaries and grain size distribution histograms for ShAPE processed Mg-4W tubes and Mg-5W rods are presented in Figure 5.

Table 2. Average grain size diameter of Mg-W precursors and ShAPE processed samples obtained at the as-forged, intermediary, and final extrudate locations using EBSD mapping.

| Specimen | Sample location | Average Diameter (μm) | Standard Deviation (μm) | Maximum Diameter (μm) | # Grains Sampled |
|-----------------|-----------------|------------------------------------|--------------------------------------|------------------------------------|------------------|
| Mg-4W precursor | As-forged | 13.6 | \pm 15.7 | 126.0 | 573 |
| Mg-4W tube | Intermediary | 2.88 | \pm 2.44 | 15.0 | 224 |
| Mg-4W tube | Final extrudate | 1.09 | \pm 0.80 | 4.0 | 187 |
| Mg-5W precursor | As-forged | 8.16 | \pm 11.2 | 125.1 | 1067 |
| Mg-5W rod | Intermediary | 1.88 | \pm 1.02 | 6.0 | 1111 |
| Mg-5W rod | Final extrudate | 1.98 | \pm 1.24 | 6.1 | 92 |

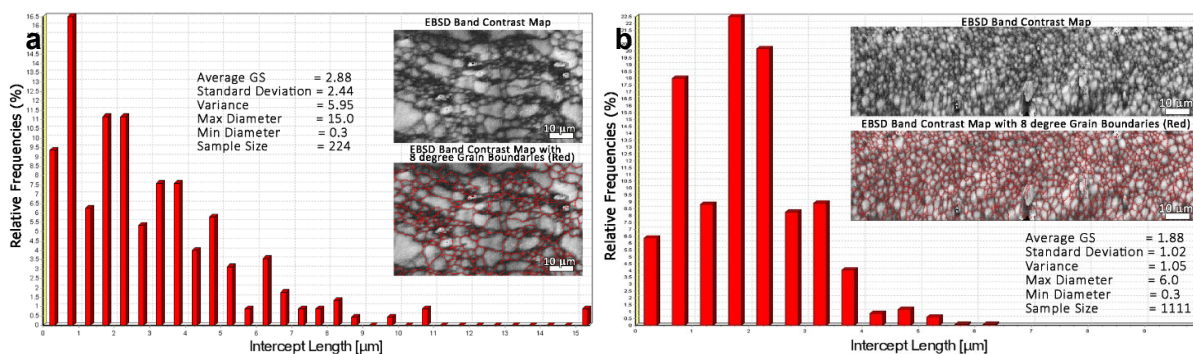


Figure 5. EBSD mapping of the location intermediary to the precursor and ShAPE processed locations of (a). Mg-4W tube and (b). Mg-5W rod. Grain size of the rod is found to be more refined than the rod at this intermediate region. The areas mapped reveal uniform grain size following ShAPE processing.

Microstructure of the ShAPE Mg-4W tube and Mg-5W rod in the earliest-to-extrude location exhibits a $<5 \mu\text{m}$ average grain size (GS). At this intermediate location in processing, the tubing material was found to have similar sizes ($\sim 3 \mu\text{m}$ for the tube and $\sim 2 \mu\text{m}$ for the rod). The tube grain size in the intermediary location demonstrated larger deviation; on the other hand, the rod material exhibited a comparatively lower deviation in average grain diameter and therefore, a relatively more uniform grain size.

ShAPE processed Mg-4W tubing and Mg-5W rod materials were evaluated in a location corresponding to a steady state processing condition, referred to as the final extrudate in Table 2. In both samples, the reported grain size was measured at the center of the extrudate. EBSD pattern quality maps with overlaid grain boundaries along with corresponding grain size histograms associated with this measurement are presented in Figure 6. In the steady state condition, the tubing exhibited a more refined grain size distribution of $\sim 1 \mu\text{m}$, with a maximum grain size of $4 \mu\text{m}$ in the evaluated region. The extrudate rod geometry had a maximum grain

size $<6.5 \mu\text{m}$ and an average grain size of $\sim 2 \mu\text{m}$. Both specimens were found to have an average grain size $<2 \mu\text{m}$, irrespective of the processing parameters used during the SHAPE process.

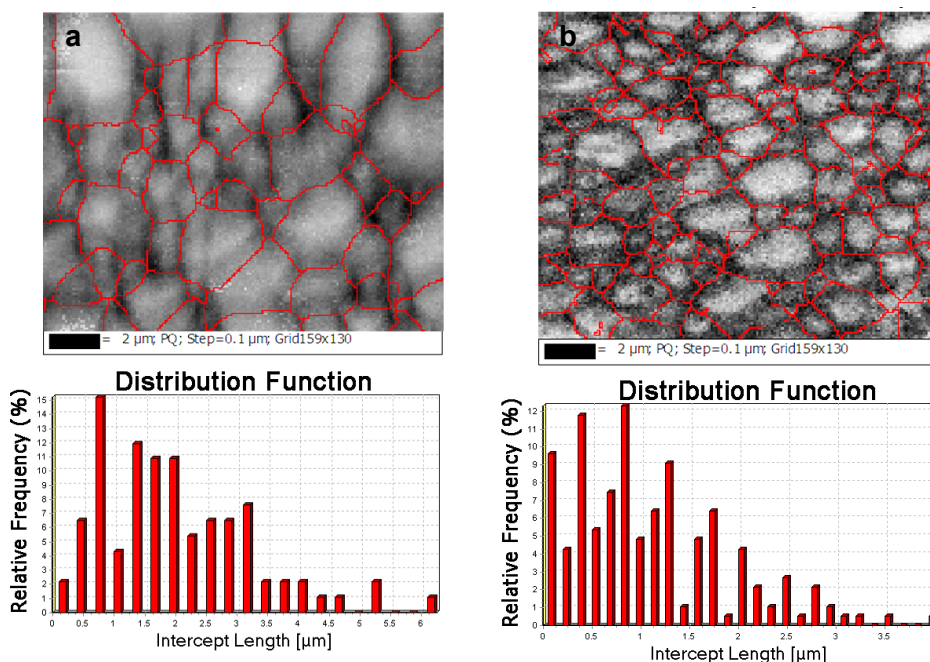


Figure 6. EBSD band contrast and grain size histograms of (a). Mg-4W tube and (b). Mg-5W rod extrudates, showing an average grain size less than $2 \mu\text{m}$.

A fore scatter image of the as-cast WJ11 is presented Figure 7 shows the Mg-rich grains in gray surrounded by a white phase believed to be intermetallic. This is further clarified with a fore scan diode montage in Figure 7 which shows dark gray grains surrounded by a white phase. Phase mapping shows the Mg-rich phase in red surrounded by $\text{Mg}_{17}\text{Sr}_2$ intermetallic in blue. The EBSD IPF-Z map indicates weak texture in what is likely to be a randomly oriented grain structure of the cast WJ11. The grain structure analysis (Figure 6) indicates that the cast Mg-rich grains range from ~ 1 to $138 \mu\text{m}$ with a mean of $\sim 20 \mu\text{m}$ with a standard deviation of $25.6 \mu\text{m}$. Not shown in the figure is that further analysis of the intermetallic phase suggests an average size of $14 \mu\text{m}$ and average pore size of $7 \mu\text{m}$.

Figure 8 shows EBSD analysis of a conventionally extruded WJ11 sample with the grain size refined to an average of $2.7 \mu\text{m}$. Dark regions aligned in the horizontal may be second phase stringers or possibly grains that were too small to be resolved with the settings used for analysis. Texture analysis shows a slight propensity of (0001) planes to align near the extrusion direction with a multiple of uniform distribution (MUD) of 6.1. EDS analysis in Figure 8 shows that Y and Zr is in solution with Mg; a few precipitates composed of Y and Zr appear to be less than $5 \mu\text{m}$. Sr appears prevalent as precipitates in the size less than $5 \mu\text{m}$ and may be aligned to some degree in the extrusion direction.

The EBSD analysis of SHAPE extruded rod of WJ11 is shown in Figure 9. The extrusion direction is vertical for these images. The grain size observed in these samples ($2 - 3 \mu\text{m}$) is smaller than the as-received cast WJ11 ($<5 \mu\text{m}$) and on par with the conventionally extruded samples. Images from EDS analysis show that lesser prevalence of Y and Zr based precipitates in the Mg matrix. While a few Sr-rich precipitates are seen in the EDS images, their density at this magnification is

much lower than those observed in cast and conventionally extruded samples shown in Figures 7 and 8.

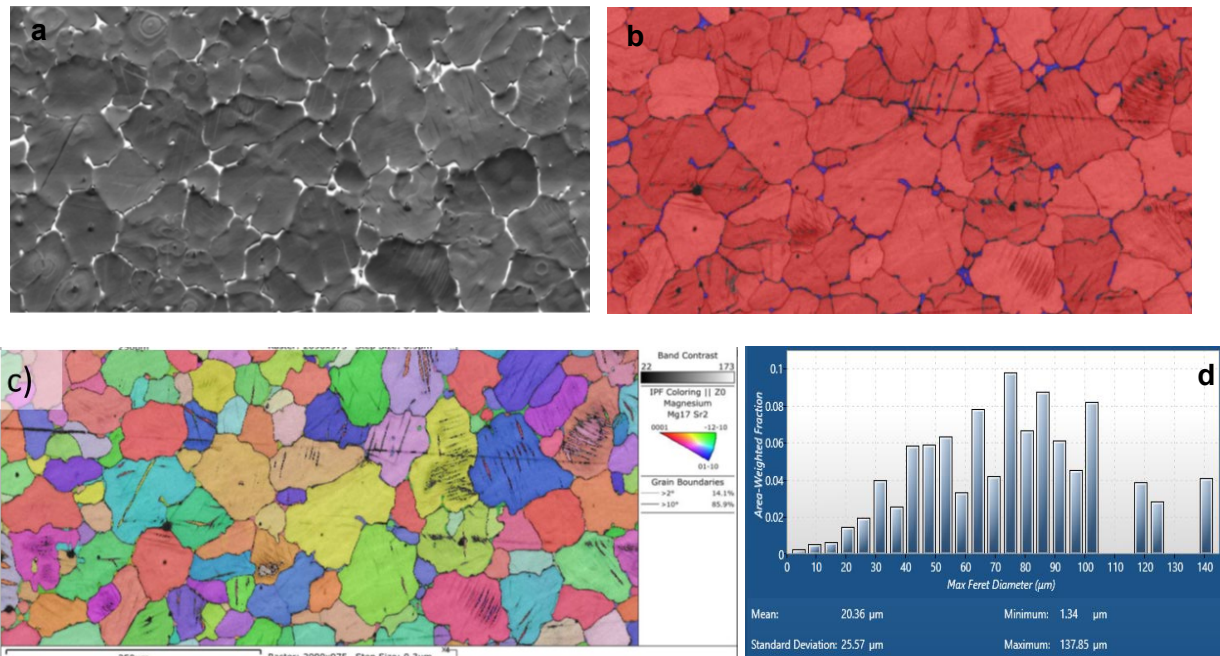


Figure 7. (a). A fore scatter image montage of as-received cast WJ11 showing expected Mg-rich phase as dark gray and second phase particles as white near grain boundaries, (b). Phase mapping confirms the Mg-rich phase shown in red and Mg₁₇Sr₂ intermetallic particles at the grain boundaries shown in blue; (c). EBSD IPFZ map showing a random texture in the as-cast WJ11 precursor billet; (d). EBSD generated area weighted fraction of grains showing an average grain size of 20 μm.

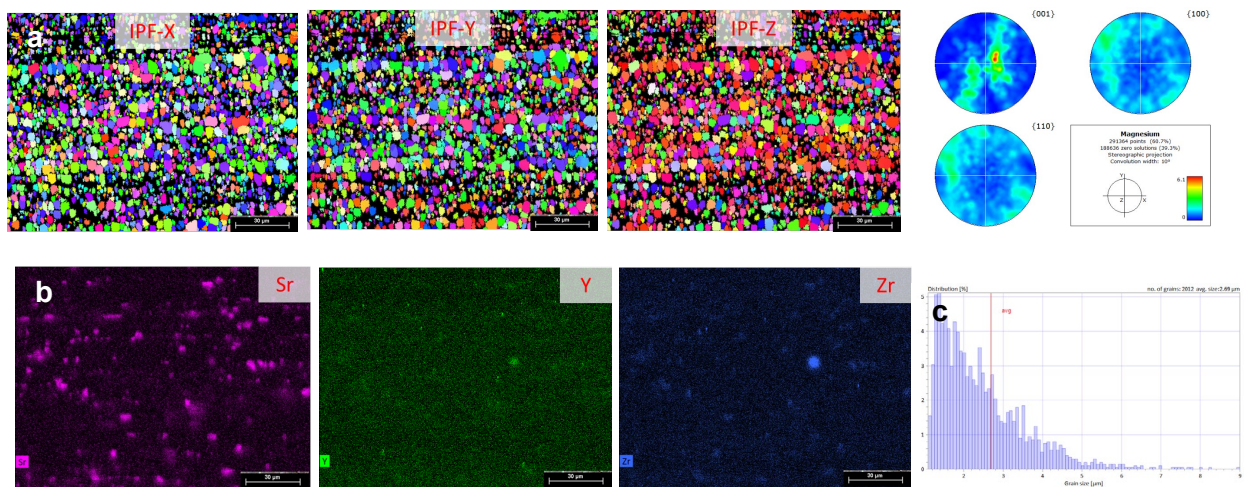


Figure 8. (a). EBSD map of as-received extruded WJ11 showing a slight texture of (0001) and potential second phase 'stringers'; (b). EDS maps of the as-received, extruded WJ11 showing precipitates comprised predominantly of strontium with an average size of ~2 μm; (c). grain size distribution histogram of cast WJ11 specimen showing an average grain size of 2.7 μm.

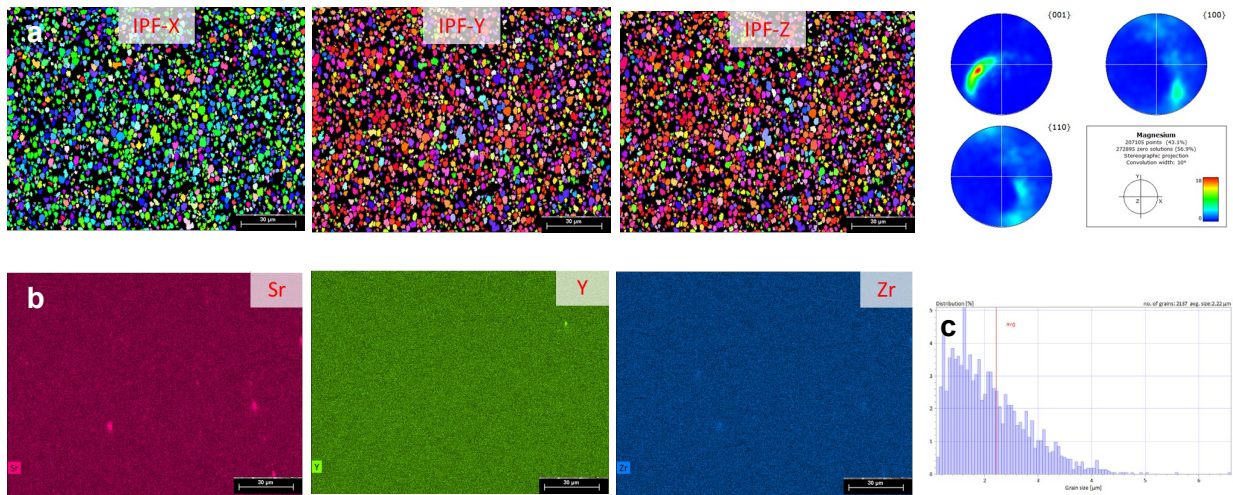


Figure 9. (a). EBSD map of ShAPE WJ11; (b). EDS maps of ShAPE WJ11 showing minimal precipitate density; (c). grain size distribution histogram of ShAPE WJ11 specimen showing an average grain size of 2.2 μm.

Since Sr does not demonstrate solubility in Mg, the EBSD and EDS results in Figure 9 from the ShAPE WJ11 analysis suggests that the Sr-rich phase is likely to be seen at finer scale. Thus, TEM analysis was performed on the extruded and ShAPE WJ11 samples and the results are shown in Figure 10.

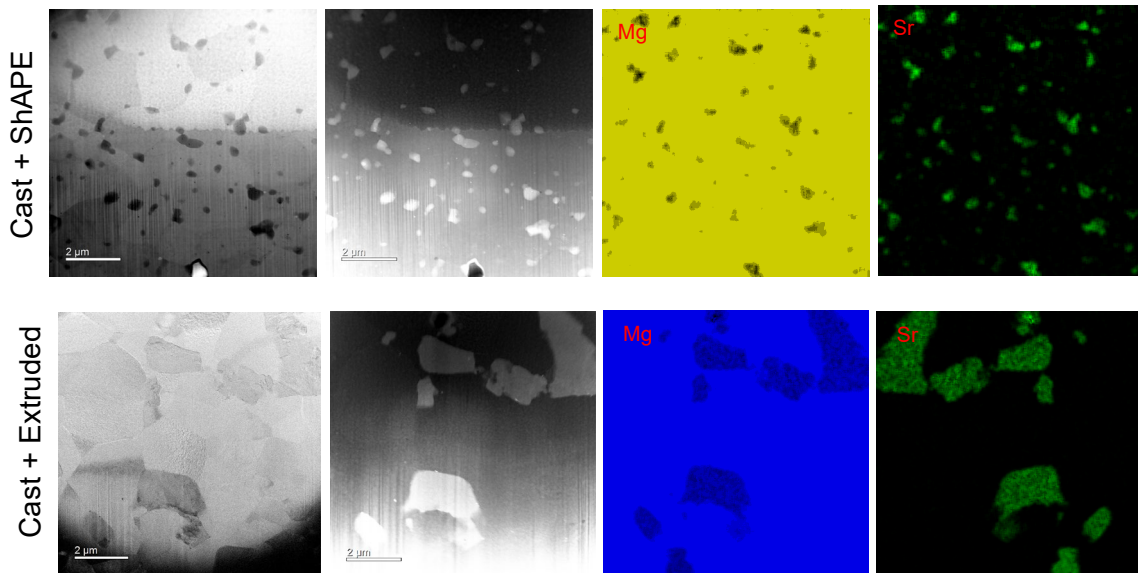


Figure 10. TEM images of ShAPE WJ11 confirming the presence of Sr-rich precipitates with an average size of <math><1 \mu\text{m}</math> in the Mg matrix; Y and Zr-rich precipitates were unobserved in the ShAPE WJ11 samples.

The BSE images of ShAPE WJ11 confirm Mg grains have an average size of 1 – 2 μm as determined by the SEM images; similar grain sizes are also seen in the extruded WJ11 samples. Interestingly, the FSD images show that there is a high density of nanoscale second phase

particles distributed across the microstructure but occurring predominantly at the grain boundaries in the ShAPE WJ11 sample. EDS analysis also shown in Figure 10 confirms that the second phases are comprised predominantly of Sr and a small amount of Zr. On the other hand, the extruded samples show larger second phases in the FSD images, with an average size of 2 – 4 μm . ESD shows that the second phases are comprised of Sr predominantly as in the case of ShAPE samples, albeit at a larger scale.

3.2 Processing Conditions

Figure 11 presents the extrusion forces experienced by the billets during ShAPE of Mg-4W, Mg-5W and WJ11 rods and tubes as a function of the tool position with respect to the billet. The load sensors and thermocouple did not record apt data during the ShAPE of WJ11 tubes and that information is not available for discussion currently.

It is evident from the results that WJ11 rods required much higher forces during ShAPE compared to Mg-4W and Mg-5W rods; this may be attributed to the higher volume fraction of precipitates and second phases in WJ11 and the consequently higher flow stresses that had to be overcome prior to material extrusion. On the other hand, despite the ShAPE processing of tube samples had a much higher extrusion ratio, similar extrusion forces were observed processing of rods and tubes for the dissolvable composites. It was also seen that the dissolvable composites demonstrated a two-stage trend in breakthrough forces where a peak was first observed, and then was followed by a smaller second peak. This trend was not seen in WJ11 where only one breakthrough force peak was identified. The two-stage trend was seen during both rod and tube manufacturing; however, the second peak was not as drastic for tube manufacturing.

Interestingly, rods were observed to be manufactured at much lower temperatures compared to tubes. Mg-4W rod was manufactured at around 350 – 380 $^{\circ}\text{C}$ while the tubes were extruded at a higher temperature of ~ 430 $^{\circ}\text{C}$. Similarly, Mg-5W rods were obtained at ~ 350 $^{\circ}\text{C}$ which was much lower than the tube extrusion temperatures of about 450 – 470 $^{\circ}\text{C}$. On the other hand, WJ11 rods were manufactured at much higher temperatures compared to the Mg-4W and Mg-5W.

3.3 Mechanical Performance

Table 3 below presents the yield strength and ultimate tensile strength of WJ11 cast samples that were extruded, and ShAPE processed for comparison. Cast and extruded WJ11, manufactured with an extrusion ratio of 10, demonstrated a yield strength of 109 MPa and an ultimate tensile strength of 178 MPa. In comparison, ShAPE processed WJ11 that were manufactured from cast precursors with an extrusion ratio of ~ 40 , demonstrated a yield strength of 163 MPa which is nearly 50% higher than the cast and extruded sample. ShAPE WJ11 demonstrated an ultimate tensile strength of 188 MPa, which is comparable to that of extruded WJ11 corresponding to a slight increase of 5.6%. Additionally, it is interesting to note that the ratio of compressive yield strength to tensile yield strength, referred to as yield asymmetry (YA), is 1.04 for the ShAPE WJ11, while the strength differential (SD), the ratio of ultimate compressive strength to ultimate tensile strength was seen to be 1.30.

It has to be noted that the research team was informed by Fortek that the Mg-4W and Mg-5W ShAPE samples demonstrated low corrosion performance despite the development of microstructures that are favorable for enhanced corrosive behavior, especially in oil and gas extraction environments. Subsequently, those samples were not tested for mechanical performance.

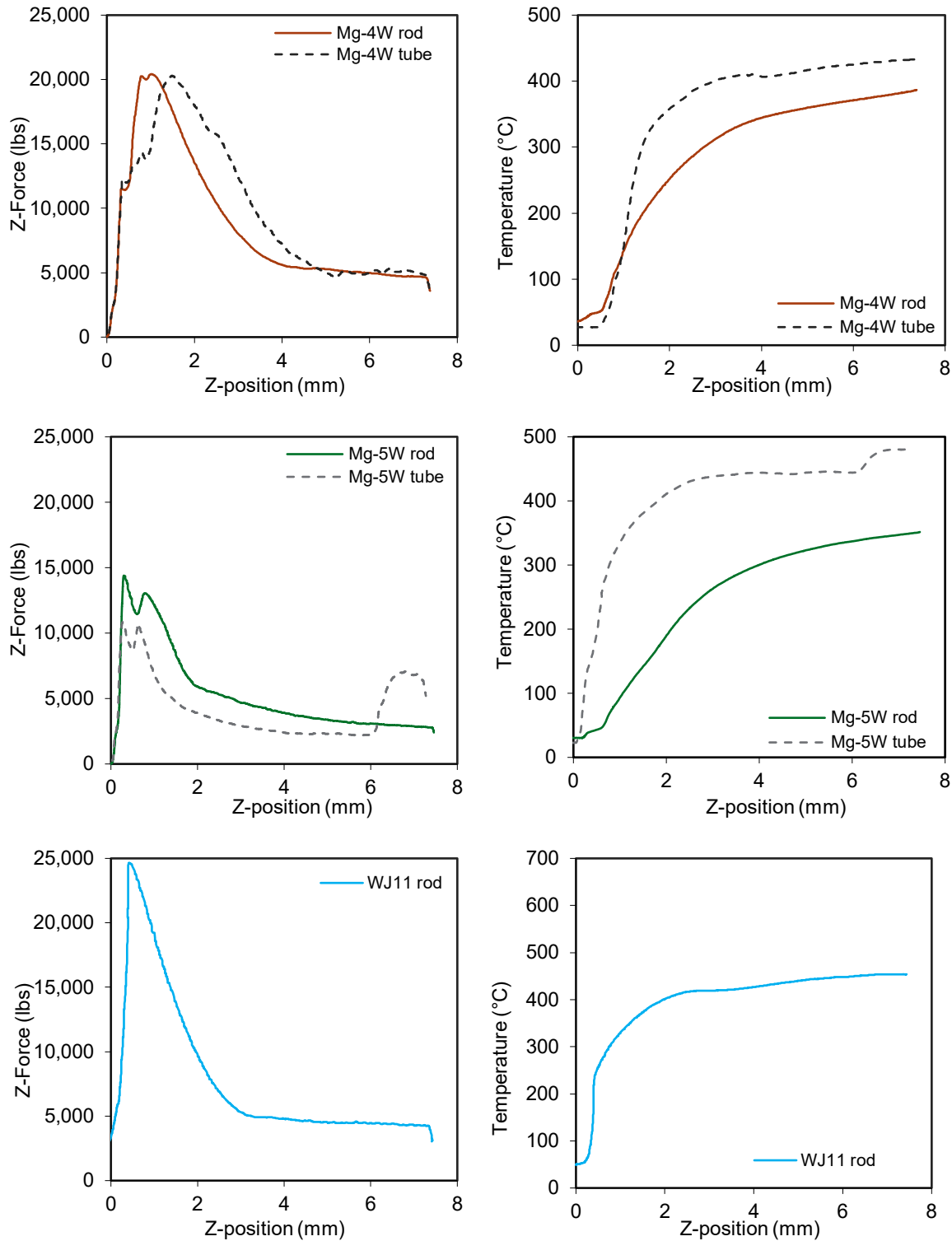


Figure 11. Extrusion forces and temperatures observed during the ShAPE of Mg-4W, Mg-5W and WJ11 rods and tubes. The legends in individual plots provide information of the sample whose data is presented in each plot.

Table 3. Mechanical properties of WJ11 samples that were ShAPE processed from cast precursors under tensile and compressive conditions. Tensile properties of cast and extruded WJ11 samples are also provided for comparison; compressive properties were unable for reporting.

| Process type | Property | Testing mode | Value (MPa) |
|-----------------|-------------------------------|--------------|-------------|
| Cast + Extruded | Yield strength | Tensile | 109 ± 7 |
| | Ultimate tensile strength | Tensile | 178 ± 1 |
| Cast + ShAPE | Yield strength | Tensile | 163 ± 19 |
| | Yield strength | Compressive | 170 ± 5 |
| | Ultimate tensile strength | Tensile | 188 ± 11 |
| | Ultimate compressive strength | Compressive | 244 ± 4 |

4.0 Conclusions and Future Work

In this work, the viability of manufacturing dissolvable alloys and composites typically suitable for applications in oil-and-gas as well as biomedical sectors were explored. This study was performed in collaboration with Fortek Inc. and University of Pittsburgh. Magnesium alloys with tungsten additives, Mg-4W and Mg-5W that were hot forged from magnesium alloy and tungsten powders were provided for this research by Fortek. University of Pittsburgh contributed cast billets and extruded rods of WJ11, a custom developed alloy with biocompatible second phase additions such as yttrium and strontium.

This study showed that 5-mm-diameter rods and 10-mm-inner diameter, 1.5-mm-thick wall tubes could be manufactured using dissolvable composites Mg-4W and Mg-5W as well as dissolvable alloy WJ11. ShAPE rods were manufacturable at comparatively lower temperatures than ShAPE tubes in general. WJ11 rods required higher temperatures and higher extrusion forces than the Mg-4W and Mg-5W composite rods.

Multimodal microstructural analysis showed that ShAPE processed Mg-4W tube and Mg-5W rod demonstrated an average grain size of 1 – 2 μm irrespective of the final form. This was a $\sim 85\%$ decrease in grain size for the ShAPE components compared to the hot-forged precursors. On the other hand, ShAPE WJ11 demonstrated similar grain size of $\sim 2 \mu\text{m}$ as hot-extruded samples, which was dramatically lower than that of the cast precursors. In all these samples, the second phase precipitates originally segregated in the composite or alloy microstructures at magnesium grain boundaries were homogeneously redistributed in the ShAPE components as sub-micron scale particles. Mechanical performance testing showed that ShAPE processed WJ11 demonstrated a yield strength of 163 MPa which is nearly 50% higher than the cast and extruded sample. On the other hand, ShAPE WJ11 demonstrated an ultimate tensile strength of 188 MPa, which is comparable to that of extruded WJ11 corresponding to a slight increase of 5.6%. These results confirm that ShAPE processed dissolvable alloy and composite materials demonstrate microstructures that are improved over their as-cast or as-forged precursors. ShAPE samples also demonstrate equivalent in some cases or much improved mechanical performance over dissolvable alloy composites that are manufactured using traditional processes.

This study was the first ever demonstration of a single-step synthesis of magnesium based dissolvable alloy and composites. ShAPE technology presents a low-carbon, sustainable, low energy pathway for manufacturing magnesium-based components that retain their structural performance during the lifetime of the component and then are dissolved in the corrosive environments they are deployed. To facilitate further development and eventual commercial deployment of such dissolvable components, it is essential to test their corrosive performance in environments where they are used typically. Additionally, it is also necessary to co-optimize material design and manufacturing windows to identify alloy and composite formulations that result in the desired combination of highest mechanical strength, ductility and tailorable sorptivity or corrosion behavior. Subsequently, it is a requirement to demonstrate preservation of microstructural features and performance of the components at pilot and commercial scales and when deployed in relevant environments. Finally, there is a need for comprehensive technoeconomic and life cycle analysis to determine the effectiveness of ShAPE in manufacturing dissolvable alloy and composite components for use in oil-and-gas, biomedical and other suitable applications.

References

1. Di Marco, C., et al., Drug-Eluting Bioabsorbable Magnesium Stent. *Journal of Interventional Cardiology*, 2004. 17(6): p. 391-395.
2. Chou, D.-T., et al., Corrosion and bone healing of Mg-Y-Zn-Zr-Ca alloy implants: Comparative in vivo study in a non-immobilized rat femoral fracture model. *Journal of Biomaterials Applications*, 2019: p. 0885328219825568.
3. Orlov, D., et al., Improvement of mechanical properties of magnesium alloy ZK60 by integrated extrusion and equal channel angular pressing. *Acta Materialia*, 2011. 59(1): p. 375-385.
4. Gao, J.H., et al., Homogeneous corrosion of high pressure torsion treated Mg–Zn–Ca alloy in simulated body fluid. *Materials Letters*, 2011. 65(4): p. 691-693.
5. Zheng, Y.F., X.N. Gu, and F. Witte, Biodegradable metals. *Materials Science and Engineering: R: Reports*, 2014. 77: p. 1-34.
6. Zeng, Z., et al., Magnesium extrusion alloys: a review of developments and prospects. *International Materials Reviews*, 2019. 64(1): p. 27-62.
7. Zhang, X., et al., Improvement of mechanical properties and corrosion resistance of biodegradable Mg–Nd–Zn–Zr alloys by double extrusion. *Materials Science and Engineering: B*, 2012. 177(13): p. 1113-1119.
8. Jamalian, M., et al., Microstructure and Texture Evolution of Magnesium alloy after Shear Assisted Processing and Extrusion (ShAPETM). *IOP Conference Series: Materials Science and Engineering*, 2018. 375: p. 012007.

Pacific Northwest National Laboratory

902 Battelle Boulevard
P.O. Box 999
Richland, WA 99354
1-888-375-PNNL (7665)

www.pnnl.gov